Vol. 24, No. 2(2025) IE25411
Revista Mexicana de Ingeniería Química

Numerical and experimental study of air heating solar collector constructed of aluminum tube pipes

Estudio numérico y experimental de un colector solar de calentamiento de aire construido con tubos de aluminio

A. López-López[1], I. A. García-Montalvo[2], S. Sandoval-Torres[3], E. Hernández-Bautista[1]*
[1]Departamento de ingeniería química y bioquímica, Tecnológico Nacional de México/ Instituto Tecnológico de Oaxaca, Oaxaca 68033, México.
[2]División de Estudios de Posgrado e Investigación Tecnológico Nacional de México/ Instituto Tecnológico de Oaxaca, Oaxaca 68033, México.
[3]Instituto Politécnico Nacional, CIIDIR Unidad Oaxaca, Santa Cruz Xoxocotlán 71230, México
Received: September 3, 2024; Accepted: March 3, 2025

Abstract

A model was developed to simulate an air heating solar collector. A 3D geometry was proposed, consisting of nine rectangular aluminum tubes and a rectangular space between the glass cover (GC) where air flows. The spatial distribution of air velocity was simulated using a Reynolds-Averaged Navier-Stokes $\kappa - \varepsilon$ model, in steady state, to calculate the heat transfer coefficients. The energy balances in transient state were performed in the GC, aluminum absorber plate (AP) and in the fluid. The energy balance considers the heat transfer in the fluid by convection, conduction and surface radiation between the AP-GC. The energy balance in the AP used a lumped analysis and considered the heat loss due to convection between the AP and fluid and heat source due to solar radiation considering transmissivity and absorptivity. The model was used to simulate different inlet velocities. The transfer coefficients in the tubes were higher and therefore the temperature, compared to the space between GC and AP. Besides, it was found that there is an increase in outlet temperature with increasing air velocity.

Keywords: Heat transfer coefficient; Interior no slip condition; Transient analysis; Turbulent flow; Surface to surface radiation.

Resumen

Se desarrolló un modelo para simular un colector solar para calentamiento de aire. Se propuso una geometría 3D, compuesta por nueve tubos rectangulares de aluminio y un espacio rectangular entre la cubierta de vidrio (GC) por donde fluye el aire. La distribución espacial de la velocidad del aire se simuló utilizando un modelo $\kappa - \varepsilon$ de Reynolds-Averaged Navier-Stokes, en estado estacionario, para calcular los coeficientes de transferencia de calor. Los balances de energía en estado transitorio se realizaron en el GC, placa absorbente de aluminio (AP) y en el fluido. El balance de energía considera la transferencia de calor en el fluido por convección, conducción y la radiación superficial entre la AP-GC. El balance de energía en la AP utilizó un análisis agrupado y consideró la pérdida de calor por convección entre la AP y el fluido y la fuente de calor por radiación solar considerando transmisividad y absortividad. El modelo se utilizó para simular diferentes velocidades de entrada. Los coeficientes de transferencia y la temperatura en los tubos fueron más altos, en comparación con el espacio entre GC y AP. Además, se encontró que hay un aumento en la temperatura de salida con el aumento de la velocidad del aire.

Palabras clave: Coeficiente de transferencia de calor; Condición interior no deslizamiento; Estado transitorio; Flujo turbulento; Radiación superficie a superficie.

*Corresponding author. E-mail: Bautistahe@gmail.com ;
https://doi.org/10.24275/rmiq/IE25411
ISSN:1665-2738, *issn-e*: 2395-8472

1 Introduction

The rapid population growth and increasing demand for energy in developing countries exposes concerns such as poverty, pollution, health, and environmental problems (Ndukwu *et al*. 2023). For this reason, these countries need modern energy to increase production, generate income and promote social development, as well as to address the health problems caused by the use of fossil fuels (Shahsavari y Akbari 2018). Currently, sustainable alternatives are being developed, such as biofuel production for energy-intensive processes (Mota et al. 2025; Romero-Bonilla et al. 2025), which generate an average energy output of 37 MJ/kg. In contrast, for low-temperature processes, solar drying plays a crucial role in achieving sustainable development goals in rural Mexican communities, as it is the most viable preservation technology for certain agricultural products (Messina *et al*. 2022).

Drying is a highly energy-intensive operation, consuming 6 to 30 times more energy than cooling and freezing depending on temperature conditions, which requires a large amount of fossil fuel consumption that generates carbon emissions into the atmosphere (Ndukwu *et al*. 2023). The use of renewable energy has the benefit of reducing dependence on these fuels and reducing carbon emissions into the atmosphere.

Global warming has increased the demand for renewable energy sources, making solar radiation the most abundant and cleanest energy source available today. In recent years, solar collector technology has developed rapidly and has been widely applied. However, solar energy is intermittent with low energy density and easy to be affected by climatic factors, which has an impact on the low solar energy use efficiency of the collector (Xiao *et al*. 2022). Therefore, technological improvements are required, such as: 1)The incorporation of thermochemical energy storage and phase change storage (AZEEZ *et al*. 2023; Mahroug *et al*. 2021). 2) The improved spatial distribution of air within the collector and the integration of ventilation systems that help to increase the heat transfer coefficients in the absorber plate (Bolaji 2012). As well as 3) the sizing and improvements in collector geometry based on computational and CFD simulations (Rajarajeswari, Alok, and Sreekumar 2018).

The development of mathematical models describing the CFD and the heat transfer in the fluid aims to describe the process to maximize the heat transfer between the absorber plate and the air, that means that more energy as heat is transported into the fluid and consequently the outlet air temperature will be higher. In this work the fluid in the collector is air, which is commonly used for drying operations.

The $\kappa-\varepsilon$ model is one of the most used turbulence models in CFD for flat plate solar collectors (AZEEZ *et al*. 2023; Rouissi *et al*. 2021; Vivekanandan *et al*. 2020). This is relatively simple compared to other more complex turbulence models. This simplicity enhances computational, enabling quicker simulations with reduced demand on computational resources. Moreover, it effectively predicts turbulence within the fluid and vortex effects in the flow.

The collector is connected to a drying chamber (Kumar y Singh 2020; Mohana *et al*. 2020), where the air at room temperature enters the collector and leaves it at a higher temperature to enter the drying chamber. The hot air leaving the collector enters the drying chamber and passes through the material to be dried, in order to yield its sensible heat and remove the water from the material.

The solar tube collector for air heating consists of a GC, an AP and wood insulation on the bottom. Solar radiation crosses the glass cover which allows the radiation to pass through (Bakari 2018; Bakari, Minja and Njau 2014), but minimizes heat loss. This is absorbed by a flat plate inside the collector, which transfers it to the fluid. This heat is transferred to the air circulating through the collector while the insulation on the sides and bottom helps to reduce thermal losses (Lingayat *et al*. 2020), retaining the heat effectively (Tiwari 2011).

In an energy balance, the AP gains energy from solar radiation and loses it by transferring heat to the air. Due to the previously mentioned and to the thermal conductivity of the AP, we can obtain a homogeneous spatial distribution of temperatures on the AP, changing only as a function of time due to solar radiation throughout the day from 500 Wm^{-2} to 1100 Wm^{-2} (Matsumoto *et al*. 2014).

The process of heat transfer between the AP and the fluid is described by the use of energy balances between these two domains, where the concept of thermal boundary layer is involved, that is described through the convective coefficients of heat transfer between the plate and the fluid. Another phenomenon is radiation between surfaces (Alleyne and Milczarek 2015) a phenomenon in parallel with the convective mechanism.

The incoming light passes through the GC because it allows passage mainly into the short infrared. The GC is a selective barrier for different wavelengths of electromagnetic radiation. In particular, it allows the shorter wavelengths of the infrared (IR) spectrum to pass through. These short IR have higher energies and are able to easily pass through materials such as GC. This light heats the AP through which the air flows; when this material is heated, it emits longer IR radiation. When the short IR passes through the glass and reaches the aluminum within the thermal system, it absorbs this energy and increases its temperature.

As the AP is heated, it begins to emit its own thermal radiation according to Planck's law. This emission is typically at longer wavelengths known as far or long IR. The long wavelengths cannot easily pass through the same material that allowed the short IR to enter initially. So. some of this energy is trapped within the system due to the greenhouse effect created by this phenomenon: heat enters but does not leave as easily due to the selective blocking exerted by the optical properties of the transparent material. This contributes significantly to the total energy losses within the collector system.

Furthermore, the air inlet temperature varies throughout the day. Early in the day, the inlet temperature and energy flux are low, resulting in a lower outlet temperature. By midday, however, with an energy flux of 1100 Wm^{-2} and a higher inlet temperature, the outlet temperature also increases.

Some studies have been developed that consider a steady state, which takes into account that the fluid temperature remains constant at the inlet and that the energy flux absorbed by the plate also remains constant (Gopi *et al*. 2020; Jallut, Jemni, y Lallemand 1988). Consequently, a state is reached in which an equilibrium is achieved in which the amount of heat entering is the same as the amount of heat leaving It is considered to be a solution that helps to understand the problem (Bensaci *et al*. 2020) but it is distant from reality.

Because of the processes mentioned above, what is proposed in this work are a series of fundamental assumptions that help us to develop a set of equations based on energy balances that can be used to simulate the process in a non-steady state. The objective of this work is to analyze the effect of the geometry of the flat plate solar collector on the heat transfer coefficients and its effect on the temporal temperature distribution.

The first part of the work presents the development of the model, which includes considerations for geometry, conservation equations, flow equations, initial conditions, and boundary conditions. It also discusses the parameters utilized to solve these equations using finite element methods. Additionally, this section outlines the experimental procedure used to obtain temperature profiles, solar radiation data, and air velocity measurements in a solar collector.

The final section presents the experimental results, primarily focusing on simulated numerical outcomes. First, it discusses the velocity distribution within the solar collector, along with the calculation of heat transfer coefficients based on this distribution. Second, it provides a comparison between experimental and simulated results. Finally, the section presents temperature distributions within the solar collector throughout the day under various velocity conditions.

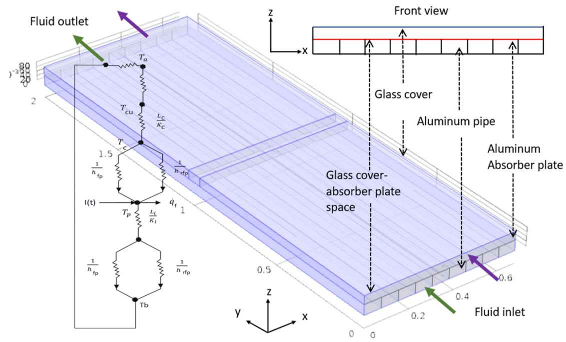

Figure 1 Geometry of flat plate solar collector for air heating and equivalent diagram of thermal resistances 1d z-direction.

2 Mathematical model

2.1 Geometry

The simulated solar collector has the dimensions of 2 m long and 0.684 m wide and consists of 9 aluminum tubes located at the bottom of the collector with dimensions of 0.076 m wide by 0.045 m high each, through which air flows. There is a space between the GCs and the AP, which is 0.684 m wide and 0.037 m high, where air also flows. The absorber plate (AP) is the upper area of the tubes exposed to solar irradiation (2mx0.684m).

The geometry does not consider the thickness of the glass cover, nor the thickness of the insulating wood on the sides of the collector and at the bottom, as these are considered as a boundary condition for thermal insulation and convective heat loss on the outer surface of the glass. Also, the thickness of the tubes is not taken into account since aluminum has a high thermal conductivity of 237 Wm^{-2} K^{-1} and a very thin thickness of less than 1 mm. In addition, these considerations reduce the solution time, since by using FEM, the mesh refinement at thin thicknesses generates many more nodes, so that the geometry of the flat plate collector is considered only as separate air sections with outer and inner boundaries. The energy transport is represented with thermal resistances separating the domains as shown in Figure 1. This diagram illustrates the heat flow in the z-direction. The environment and glass cover present a thermal resistance defined by an overall heat transfer coefficient, ho. Between the glass cover and the absorber (AP), there are resistances due to convection within the fluid (h_{fp}) and radiation (h_{rpf}) between the surfaces. Additionally, within the tubes, there is resistance due to fluid convection (h_{fp}). In this diagram, solar radiation affects the temperature T_p, modulated by the absorptivity and transmissivity of the materials.

2.2 Model assumptions

In order to reduce the complexity of the model and focus on the phenomena of interest, the following major assumptions were considered, some other assumptions will be considered during model development.

- Air is considered as an incompressible fluid
- The air fluid presents a fully developed turbulent flow distribution pattern.
- There is no temperature gradient in the thickness and length of the glass cover and absorber plate (Al-Tabbakh 2022).
- The temperature of the absorber plate varies as a function of time, but not of space, so a global analysis of heat transfer is possible.
- The heat lost at the side boundaries is negligible.
- The absorptivity of solar radiation on the glass cover is negligible.
- Forced convection is present, therefore the velocity distribution remains steady state during operation.

2.3 Conservation equations

2.3.1 Air velocity distribution in the solar collector

The working fluid is considered as air, as an incompressible fluid with 11 % relative humidity. Air was introduced into the collector (Figure 1) with an average velocity at the inlet in the y-direction of 1.5 m s^{-1}, 2 m s^{-1} and 2.5 m s^{-1}. All these conditions start from zero, these velocities generate a turbulent distribution pattern, with Reynolds number greater than 4000, as will be shown below.

Equation 1 is the modified Navier Stokes equation for Reynolds average Reynolds number (RANS) and the turbulent distribution parameters are $\kappa-\varepsilon$. Because in the assumptions we have that the distribution does not change with temperature, this equation is solved in steady state. Besides, the continuity equation (1) accompanies this equation. It expresses that the amount air mass in is the same as the air mass out.

$$\rho_f(\mathbf{u}\cdot\nabla\mathbf{u}) = \nabla\cdot\left[-p\mathbf{I}+(\mu+\mu_T)\left(\nabla\mathbf{u}+(\nabla\mathbf{u})^T\right)-\frac{2}{3}\rho_f\kappa\mathbf{I}\right]$$
$$\rho_f\nabla\cdot\mathbf{u} = \mathbf{0} \tag{1}$$

This equation models the behavior of a turbulent flow considering both viscous effects and the additional effects of turbulence. The boundary conditions at the walls of the tubes and the walls of the space between the glass and the absorber plate are non-slip conditions for the air. These are classified into inner and outer boundaries. Equation 2 shows the conditions applied to these boundaries.

$$\mathbf{u}\cdot\mathbf{n} = \mathbf{0} \tag{2}$$

2.3.2 Heat transfer coefficients

The Reynolds number was calculated once the velocity distribution generated by equation 1 was obtained. This considers an equivalent hydraulic diameter for rectangular ducts (equation 3)

$$D_h = \frac{4b_1b_2}{2(b_1+b_2)} \tag{3}$$

Where b_1 and b_2 are the height and width of the tubes and the height and width in the space between the glass cover and the absorber plate. Therefore, there will be two different equivalent diameters, one for the tubes and one for the space between AP and GC.

The Reynolds and Prandtl number are calculated at an average temperature of the fluid air in the collector, initially proposed. This will be modified when the energy balance will be solved, until the value will be obtained by successive approximations. These values are used in the following expression to calculate the Nusselt number (Bensaci *et al*. 2020).

$$Nu = \frac{h\cdot D_h}{k} = 0.023Re^{0.8}Pr^{0.4} \tag{4}$$

This expression is used to calculate the heat transfer coefficients inside the tubes and in the space between the glass cover and the absorber plate.

The radiation transfer coefficient (Tiwari 2011) between the absorber plate and the glass cover in °C, uses the average temperatures of T_p and T_c, also proposed initially and obtained by successive approximations as well.

$$h_{rpc} = \varepsilon_{eff}\sigma\frac{\left[{T_p}^4-{T_c}^4\right]}{T_p-T_c} \tag{5}$$

Where σ value 5.67x10^{-8} $Wm^{-2}K^{-4}$ is the Stefan-Boltzmann constant and $?_{eff}$ is the effective emissivity of the glass-plate system and is given as follows.

$$\varepsilon_{eff} = \left[\frac{1}{\varepsilon_p}+\frac{1}{\varepsilon_c}-1\right]^{-1} \tag{6}$$

2.3.3 Kinetics of temperature on the absorber plate

Because aluminum is a material with a high thermal conductivity (237 $Wm^{-1}K^{-1}$) and very thin thickness (1 mm). Also, the convective heat transfer coefficients range from 8 to 18 $Wm^{-2}K^{-1}$, giving us a Biot number « 1(Ranmode, Singh, Bhattacharya 2019). Furthermore, the absorber plate is subjected to an energy flux during operation that goes from 550 to 1100 Wm^{2-2}, it can be considered that the absorber plate has a uniform temperature distribution profile that only varies as a function of time. Therefore, a lumped analysis can be performed(Al-Tabbakh 2022). The system is divided into a number of discrete "lumps" and assumes that the temperature difference within each lump is negligible. This approximation is useful for simplifying otherwise complex differential heat equation.

$$\rho_p C_{p_p} d_p \frac{\partial T_p}{\partial t} = \alpha \tau I(t) - h_{fp}\left(T_p - T_f\right) - h_{rpc}\left(T_p - T_c\right) \tag{7}$$

The energy balance in the absorber plate (equation 7) considers that the temperature variation as a function of time depends on an energy flux due to solar radiation, multiplied by the absorbance and transmissivity of the glass plate, minus the amount of energy lost by the plate due to convection from the two sides of the plate, plus the surface-to-surface radiation between the absorber plate and the glass cover, considered in the heat transfer coefficient in equation 5. These are shown in the equivalent thermal resistance diagram.

The solar radiation I(t) is a function of time, and the data were taken experimentally, they are required by the model. Besides, equation 3 being an ODE requires initial conditions, the initial value for the temperature is 18.7 °C.

2.3.4 Transient-state temperature distribution in the fluid

The energy balance in the fluid considers variations in time and space of the fluid domain. Therefore, a PDE as energy conservation equation is used for the description of this phenomenon. The conservation equation considers the mechanism of heat transfer due to conduction and convection considering the velocity distribution of equation 1.

$$\rho_f C_{p_f} \frac{\partial T_f}{\partial t} + \rho_f C_{p_f} \mathbf{u} \cdot \nabla T_f = \nabla \cdot \left(\mathbf{k_f} \nabla T_f\right) \tag{8}$$

However, to take into account, the heat transfer between the fluid and the absorber plate. As well as the fluid and the glass cover, the following boundary conditions in the fluid were considered.

2.3.4.1 Boundary condition of the energy conservation equation in the fluid

The fluid space of the glass cover and absorber plate (Figure 1) is subjected to two sources of heat. The first term represents convective heat transfer between the fluid and the GC within the space between the GC and AP. The second is due to heat gain by the fluid through the absorber plate due to convection, shown in equation 9.

$$\mathbf{n_z} q_z = h_{cf}\left(T_c - T_f\right) + h_{fp}\left(T_p - T_f\right) \tag{9}$$

The boundary condition inside the tubes is due to convection using a different heat transfer coefficient h_{fp} inside the tubes, as the equivalent diameter is modified. This energy flux depends on the fluid temperature and the plate temperature, shown in equation 10.

$$\mathbf{n_z} q_z = h_{fp}\left(T_p - T_f\right) \tag{10}$$

Furthermore, the convective boundary condition on the outer glass cover depends on the external velocity, and the ambient temperature (T_0). This was considered as the input to the solar collector at each time. This temperature is used in equation 11.

$$\mathbf{n_z} q_z = h_0\left(T_c - T_0\right) \tag{11}$$

The collector base (bottom) as well as the side faces are considered insulated, thermal insulation boundaries.

2.4 Numerical simulation

Figure 2 show the flowchart of the model solution. The model operates as follows: initially, input parameters such as solar radiation and ambient temperature are introduced. Next, the steady-state Navier-Stokes equation is solved, assuming a proposed average fluid temperature. After the velocity distribution in the collector is obtained, the transfer coefficients based on Reynolds and Nusselt numbers are calculated.

These coefficients are used to perform the transient state energy balance in the absorber plate and the fluid. If the average temperature of the fluid does not coincide with that proposed, the Navier-Stokes equation is solved again with the calculated temperature, repeating the process by successive approximations. Finally, the temperature in the plate, in the fluid and in the glass, cover is determined.

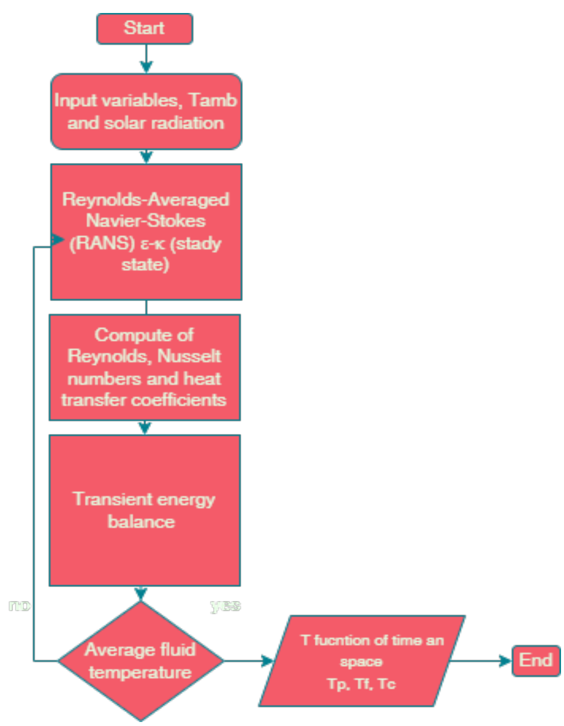

Figure 2 Flowchart of the model solution.

The model was solved using Comsol Multiphysics 4.3b, using a computer with a 3. 30 GHz and 16 Gb in Ram, equation 1 was solved for 295806 degrees of freedom, in a total time of 699s, in steady state and for equation 3 and 4, coupled transient state equations were used, using the velocity distribution of equation 1, for 45968 degrees of freedom plus 21357 internal degrees of freedom, with a time step of 60s, which gives a solution time of 589s. A mesh was created with 10269 tetrahedral elements, with mesh refinement at the corners. The size of the elements varies from 0.0513m to 0.0128m.

For the solution of the model, solar radiation, ambient temperature, and air velocity at the collector inlet are input. The output variables are the velocity distribution in the solar collector, the plate temperature as a function of time, the fluid temperature as a function of time and space, and the glass cover temperature.

2.5 Experimental data for model validation

For the data collection in the solar collector described in the previous section, a Vaisala Veritec logger and type K thermocouples of the same brand were used, with an accuracy of 0.01°C. The thermocouples were positioned as follows: one before the inlet of the solar collector (T0) to measure the ambient temperature, another in contact with the tubes (Tp) in the area exposed to solar radiation, a third at the outlet of the solar collector, measuring the air temperature in the space between the glass cover and the absorber plate (T C-P space), and the last one the outlet temperature of the tubes (Tpipe). The nomenclature in parentheses will be referenced in subsequent figures under different conditions.

Solar radiation (Sol_rad) at the collector was measured using a Fluke FLK-IRR1-SOL pyranometer, positioned at the same angle of incidence as the solar collector, which is 40°. The air velocity at the inlet was maintained at 2 m/s and measured at the outlet of the collector using an anemometer. Data acquisition spanned 6 hours, from 10 am to 4 pm in Oaxaca, Mexico.

In this operation, the controllable variables are limited. These include the air velocity and the angle of inclination of the collector. For this study, an air velocity of 2 m/s was chosen. This was because the calculation of the Reynolds number resulted in a fully developed turbulent flow distribution. On the other hand, a tilt angle of 40° was used to compensate for the lower solar radiation during winter or months with low irradiation. In addition, the steeper angle facilitates rainwater runoff and reduces the need for cleaning during the rainy season (Kramer *et al*., 2017).

3 Results and discussion

Figure 3 shows the velocity distribution in the flat plate collector in the tubes and the space between the absorber plate and the glass cover. The inlet air velocity was uniformly distributed average initial velocity. This figure shows that the velocity variation was mainly in the longitudinal direction of the collector, y-direction. This profile shows a slightly higher velocity in the tubes than in the space between the glass cover and the absorber plate. This modified the heat transfer coefficients to the fluid in each of these spaces.

Figure 3 presents the steady-state velocity distribution. In the yz-plane, it is observed that the velocity at the tube inlets corresponds to the initial values (1.5, 2, and 2.5 m/s) but increases along the y-direction due to the thermal expansion of the fluid as it is heated. This behavior was experimentally confirmed using an anemometer, which showed higher velocities at the tube outlets. Thermal expansion occurs more rapidly at higher velocities, as demonstrated in Figures 3b and 3c, where the velocity profile becomes uniform in the y-direction more quickly. Additionally, the xz-plane visualizations emphasize the no-slip condition at the tube walls and the presence of higher velocities at the center of the tube.

Higher Reynolds numbers were generated in the part of the glass cover and absorber plate (Figure 4), than in the tubes. Contrary to the fluid velocity, because the Reynolds numbers were proportional to the equivalent diameter, calculated with equation 3. The equivalent diameter of the space between the glass cover and the absorber plate was larger. This when multiplied by the properties of the fluid generates higher Reynolds numbers than in the tubes. These Reynolds numbers had values above 4000 for all cases, which confirms a fully developed turbulent flow. This is shown in Figure 4 for all velocities.

Once the Reynolds number was obtained, the Nusselt Number was calculated (equation 4). Also using the equivalent diameter, the heat transfer coefficients were calculated. However, in this case the transfer coefficients resulted proportionally inverse to this diameter, so we will have higher transfer coefficients in the tubes compared to the space between the glass cover and the absorber plate. This is also shown in Figure 4, for all simulated air velocities.

Figure 4 is consistent with the findings in Figure 3, showing that the initial inlet velocity provided by the fan increases due to thermal expansion. This velocity is accounted for in the Reynolds number and Equation 4, implying that any changes in velocity directly influence these coefficients and, consequently, the heat transfer process. Although convection coefficients are relatively low compared to other heat transfer process,

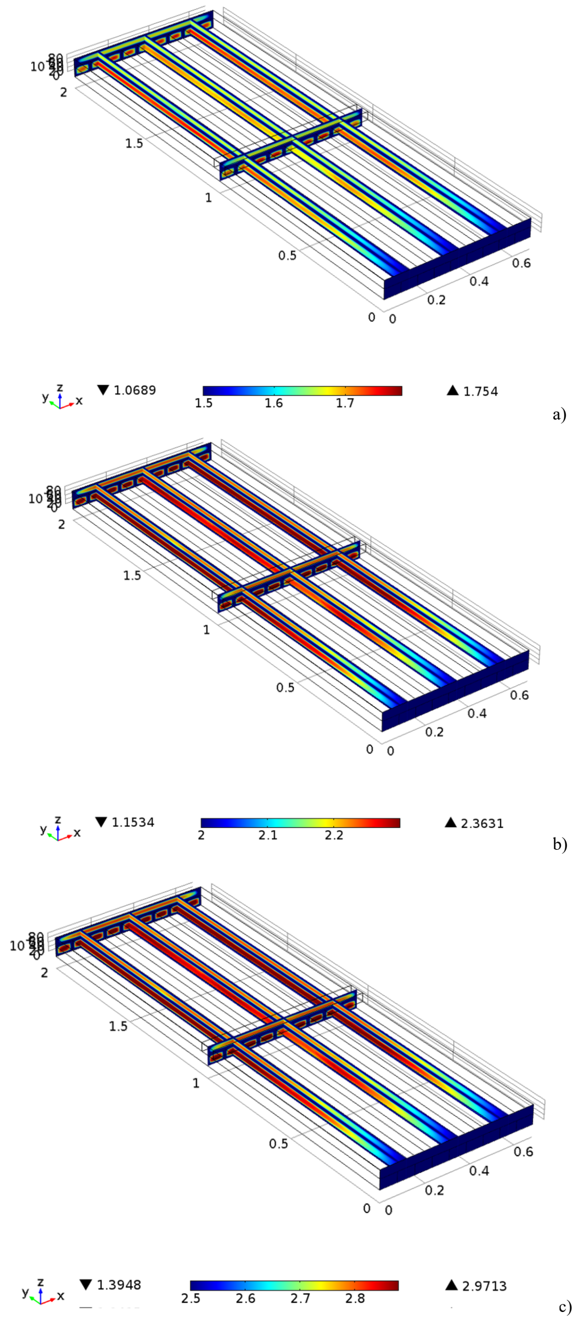

Figure 3 Velocity distribution in the flat plate solar collector a) 1.5 m s^{-1}, b)2 m s^{-1} and c)2.5 m s^{-1}.

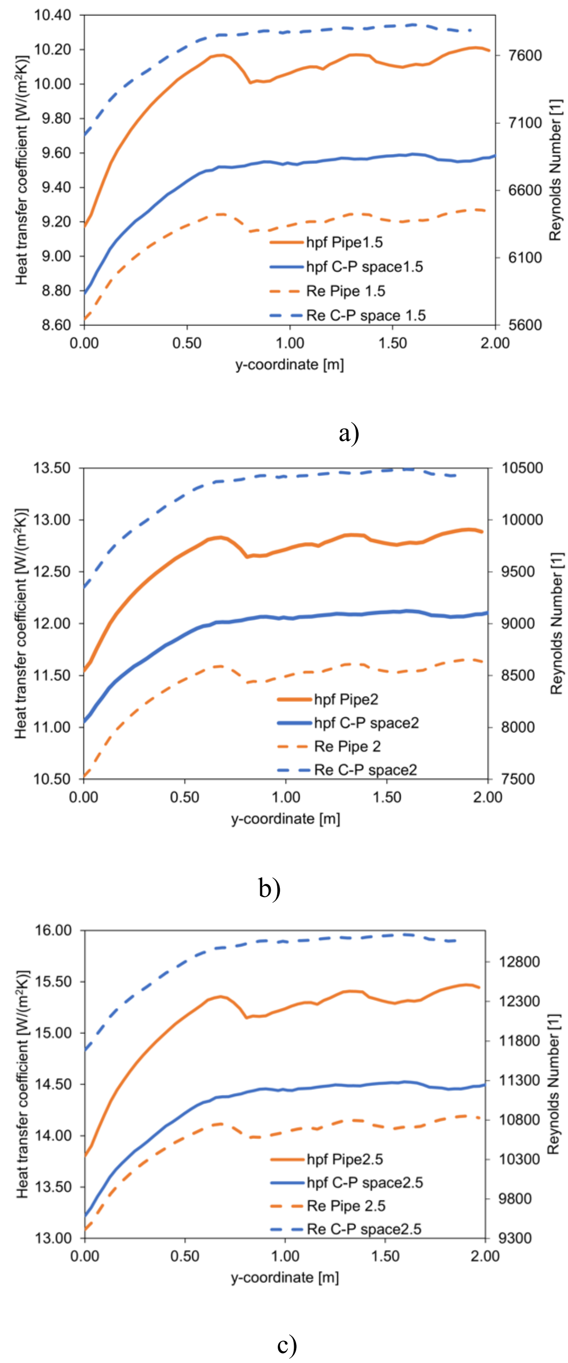

Figure 4 Reynolds number computed with velocity distribution and heat transfer coefficient between the fluid and the absorber plate at a) 1.5 m s^{-1}, b) 2 m s^{-1} and c) 2.5 m s^{-1}.

Tiwari *et al*. (2011) report even smaller values for natural convection, such as 2.847 Wm^{-2}K^{-1}. In this study, the maximum forced convection coefficient reaches 15 Wm^{-2}K^{-1}, with variations observed along the longitudinal axis of the solar collector.

Bensaci *et al*. (2020) calculated heat transfer coefficients for Reynolds numbers in the range of 2300 to 8300, using standard Dittus-Boelter correlations. The values obtained for the heat transfer coefficients ranged from 10 to 20 Wm^{-2}K^{-1}. These coefficients were observed to vary along the length of the collector, decreasing due to the presence of baffles on the absorber plate.

Figure 5 shows the temperature distribution in the solar collector at different velocities and times, the first profile is shown at 3600s, where the heating of air in the collector began, where it is shown that the heating of the air was greater in the tubes than in the space between the absorber plate and the glass cover, this behavior was the same at all velocities. As time progresses, the temperature inside the collector increases as the solar radiation I(t) (equation 9) increases. At 7200 s, the collector

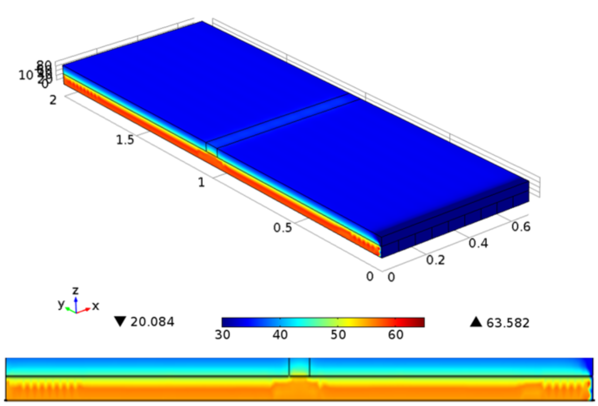
▼ 20.084
30 40 50 60
▲ 63.582

a1)

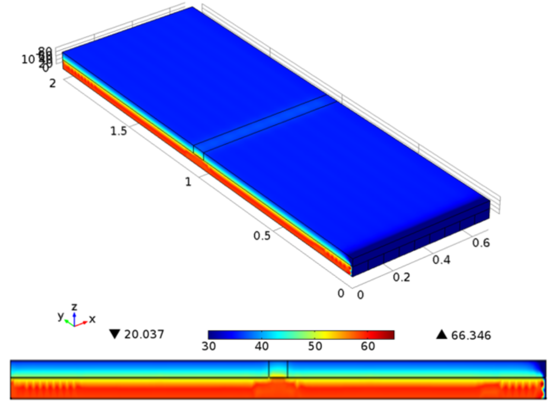
▼ 20.037
30 40 50 60
▲ 66.346

b1)

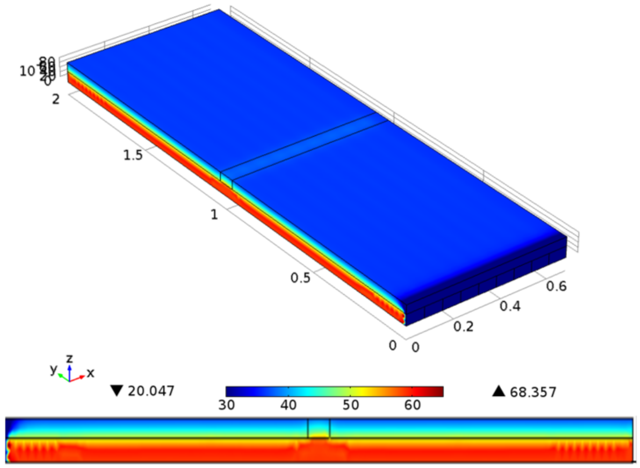
▼ 20.047
30 40 50 60
▲ 68.357

c1)

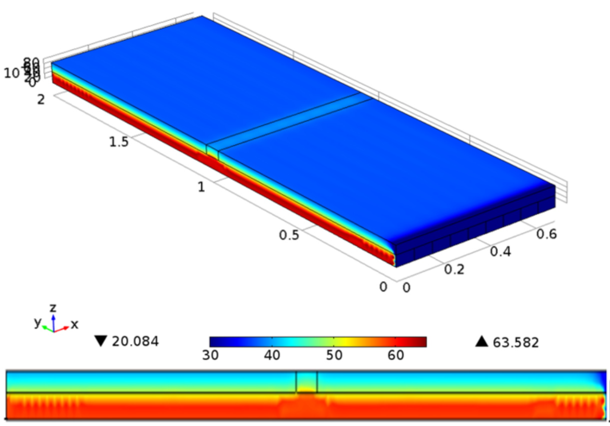
▼ 20.084
30 40 50 60
▲ 63.582

a2)

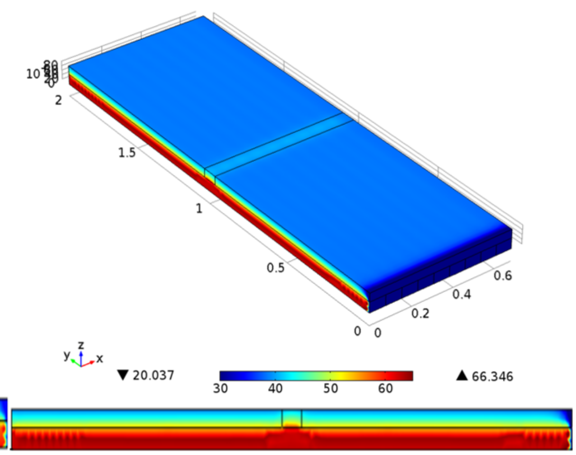
▼ 20.037
30 40 50 60
▲ 66.346

b2)

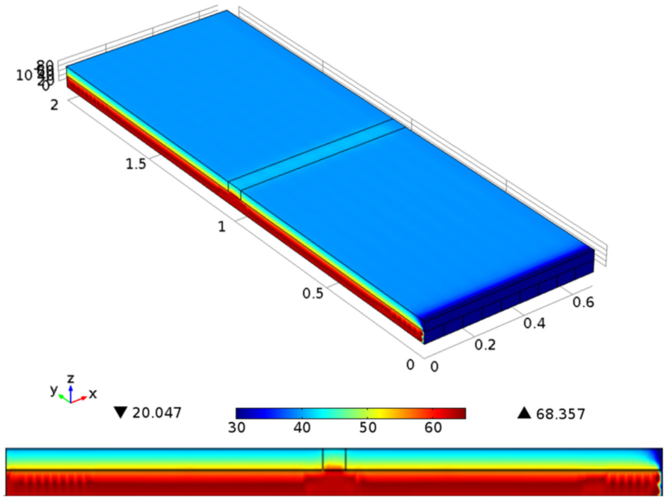
▼ 20.047
30 40 50 60
▲ 68.357

c2)

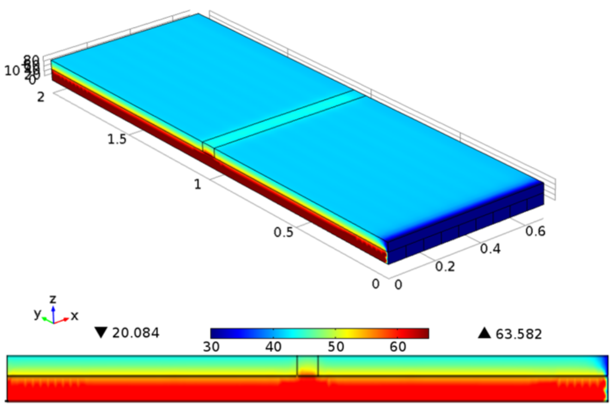
▼ 20.084
30 40 50 60
▲ 63.582

a3)

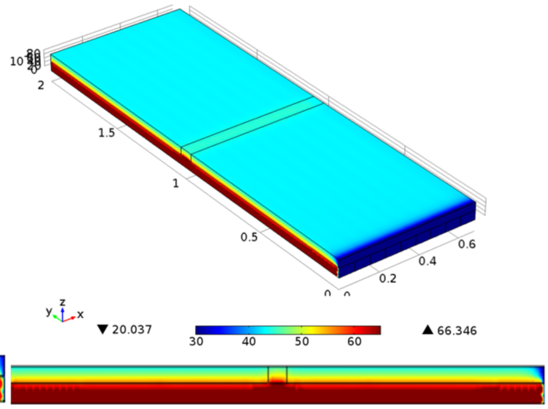
▼ 20.037
30 40 50 60
▲ 66.346

b3)

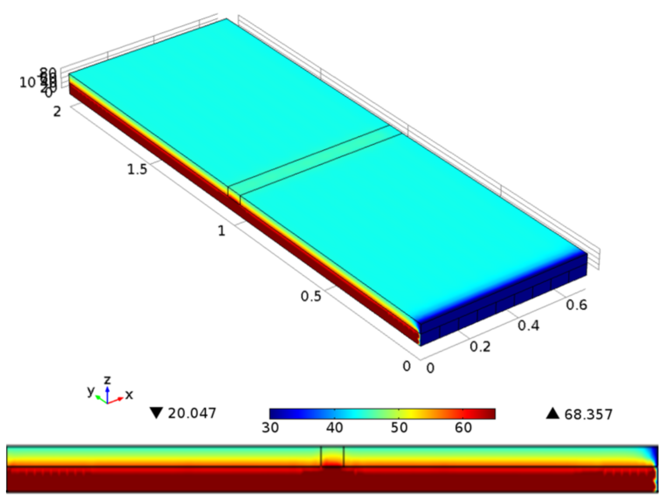
▼ 20.047
30 40 50 60
▲ 68.357

c3)

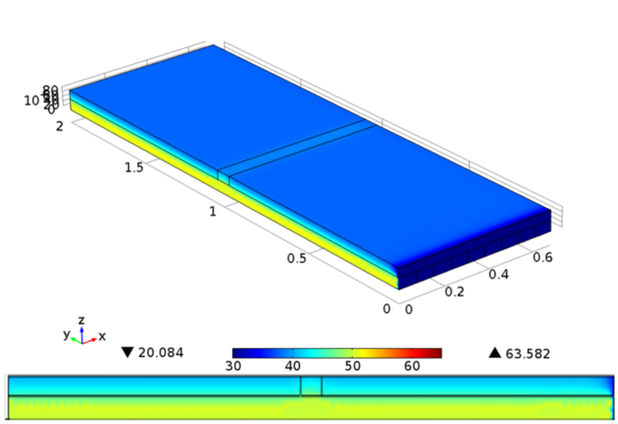

a4)

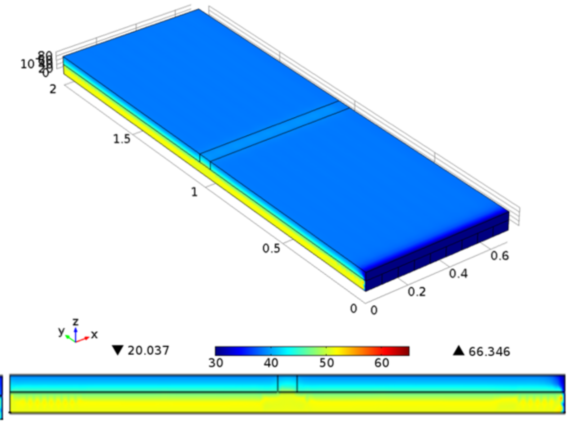

b4)

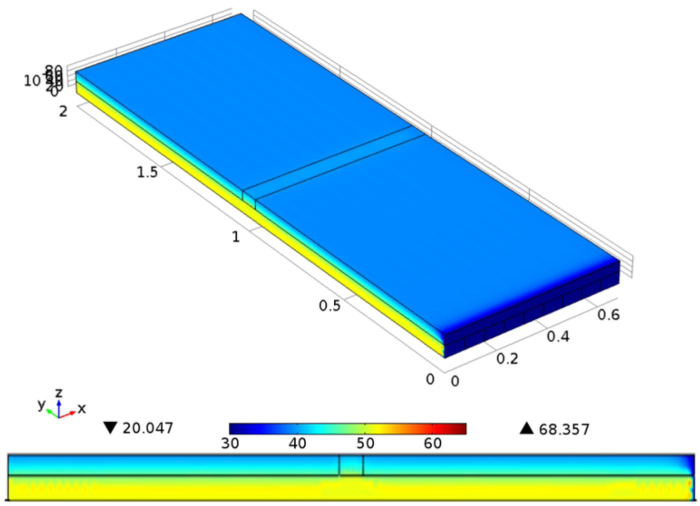

c4)

Figure 5 Temperature distribution in the flat plate solar collector, for velocities a) 1.5 m s^{-1} b) 2 m s^{-1} and c) 2.5 m s^{-1} at different times 1) 3600 s, 2)7200 s 3)15000 and 4)30600s.

temperature increased maintaining the same behavior as in the previous time, the transfer coefficient increases (Figure 4), so the temperature also increased, one of the advantages of this model is that it is possible to use the same function of solar radiation with respect to time and vary only the air velocity, keeping the other conditions constant. This is very complicated experimentally, since the solar radiation varies a lot due to the weather conditions each day.

The time of 15000 s was chosen because it was when the highest solar radiation occurs and it was at that time when the highest temperature inside the collector was obtained (Figure 5 a3,b3,c3). We can also observe that the higher the air velocity, the higher the transfer coefficients since the temperature profile was much higher. Finally, Figure 5 a4, b4 and c4 show the temperature distribution when the solar radiation decreases. Therefore, the temperature also decreases, and the model was able to capture these variations.

Figure 5 illustrates the temperature distribution in the yz-plane, showing that the temperature is higher inside the tubes compared to the space between the glass cover and the absorber plate. Due to the small variation in the coefficients, the temperature variation along the y-direction is much smaller than that along the z-direction. This indicates that the dependence of the coefficients on velocity is minimal. The temperature variation along the z-axis is more pronounced, with the highest temperatures observed at the absorber plate, represented by the horizontal line in the yz-plane that separates the space between the glass cover (C-P) and the tubes. The average temperatures of the glass cover, the air space between the glass cover and the absorber plate, the air inside the tubes, and the absorber plate were calculated and plotted as a function of time, as shown in Figure 6.

Figure 6 depicts the temperature kinetics of the absorber plate (Tp), the air within the tubes (Tpipe),

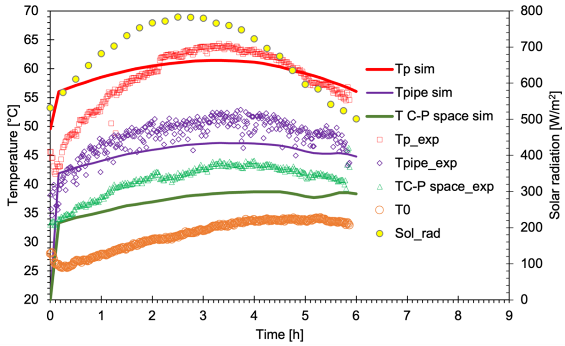

Figure 6 Experimental and simulated comparison of temperature kinetics in various sections of the solar collector operating with an inlet velocity of 2 m/s.

and the space between the glass cover and the absorber plate (T C-P space). Both experimental and simulated curves are displayed at 2 m/s. Additionally, ambient temperature and solar radiation are shown on the secondary axis; these were used as input data for the model. It is evident that the model consistently underestimates the temperature values over time, except for the temperature at the plate, where the simulated temperature is initially higher in the first few hours. These findings are attributed to the calculation of the transfer coefficients based on empirical correlations.

Figure 6 demonstrates a good agreement between the experimental and simulated data after the first hour, with a maximum discrepancy of 6 °C. The fit improves further after 2.2 hours, with the maximum difference reaching 10 °C, except for the AP temperature. The energy balance on the AP incorporates two coefficients: one for radiation (hprf) and one for convection (hpf). The convection coefficient is applied both at the top of the AP for the fluid (hpf C-P) and at the bottom (hpf Pipe). However, these coefficients tend to underestimate the energy lost from the plate, necessitating experimental calculation. The model predicts a higher temperature on the plate, which blocks the transfer of heat to the C-P space and the fluid inside the pipes, resulting in a lower simulated temperature in the pipes compared to the experimental data.

Al-Tabbakh (2022) presents a transient state study of a solar air collector with circular tubes, where a constant solar radiation is incident on the absorber plate. The results show that the highest temperature corresponds to the absorber plate, followed by the fluid, the glass cover and finally the ambient temperature. However, the temperatures reach a stationary equilibrium, as the study does not consider daily variations in solar radiation.

Rani and Tripathy (2020) analyze how different mass flow rates affect the performance of a solar air heating collector. Their results plot the temperature variation with time for the absorber plate, the fluid, the glass cover and the ambient temperature, showing similar behavior to that observed by Al-Tabbakh (2022) and this work. In addition, the mass flow, which is directly related to the air velocity, has a significant impact. In this work, it is confirmed that as the velocity increases, the absorber plate and fluid temperatures also increase, as shown in the figure below.

Table 1 presents the average energy losses throughout the day in the collector, calculated experimentally using an energy balance. It is observed that the largest amount of energy is lost at the bottom and sides of the collector, followed by the glass, where losses of 15 % occur due to transmissivity and absorptivity, in addition to a convective loss of 4 %. The table also shows the heat transfer coefficients at the surface and at the sides. It is also indicated that the average heat transfer coefficient used in the fluid and plate is 12 W/m^2 K, a value that coincides with the one used in the model for that velocity (Figure 4c). Overall, the collector achieves an efficiency of 37%, which could be improved by better insulation on the sides and by replacing the glass with polycarbonate.

Finally, in Figure 7 is shown the average temperature of the absorber plate, the fluid, the space between the absorber plate and the glass cover, the glass temperature, and the experimental ambient temperature. The absorber plate was the heat source; therefore, the temperature of the absorber plate will be higher in the solar collector, followed by the fluid temperature in the tubes where the transfer coefficients were higher and then the temperature of the space between the absorber plate and the fluid. Also, this graph also shows the ambient temperature used in these simulations.

Table 1. Efficiency and Energy Loss of Collector (Experimental Data, 2 m/s).

	Convection and radiation on the glass cover surface	Lateral and bottom of the collector	Transmission and absorption glass cover	Efficiency of the collector and heat transfer coefficient in the fluid
Loss of energy	4	44	15	37
Heat transfer coefficient	5 W/m^2 K	10 W/m^2 K		12 W/m^2 K

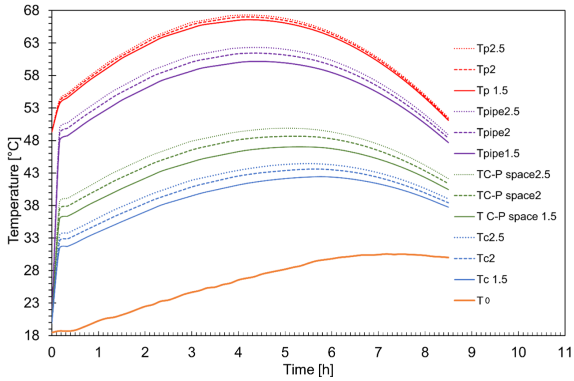

Figure 7 Temperature kinetics of the absorber plate, temperature of the air outlet of the tubes and the space between the glass cover and the absorber plate at different air flows of 1.5 m s^{-1}, 2 m s^{-1} and 2.5 m s^{-1}.

Conclusions

A model was developed to simulate heat transfer in a flat plate solar collector for air. A Reynolds-Averaged Navier-Stokes (RANS) $\kappa-\varepsilon$ model was used to obtain the velocity distribution. The energy balances in the absorber plate were modeled using a Lumped Model and a heat balance in the fluid using an PDE. The model correctly simulates the velocity distribution profile inside the collector and the temperature distribution inside the solar collector in non-steady state, taking into account the geometrical variations of the collector. The velocity distribution profile shows a velocity variation mainly in the longitudinal direction of the solar collector, y-direction.

The Reynolds numbers in the tubes resulted much smaller than in the space of the glass cover and absorber plate, so we have a higher turbulence and mixing in the part of the glass cover and absorber plate. However, the heat transfer coefficients were much lower due to the smaller equivalent diameter of the tubes which is inversely proportional to the Nusselt number.

The experimental temperature data were compared with the simulated data at a velocity of 2 m/s, showing a good fit in the fluid between the two datasets after the first hour, with a maximum difference of 6 °C. However, for the temperature on the plate, the fit improves after 2.16 hours, with a maximum difference of 10 °C.

The energy balance for the plate incorporates two coefficients: one for radiation (hprf) and one for convection. The convection coefficient is applied at the top of the plate for the fluid (hpf C-P) and at the bottom (hpf Pipe). These coefficients, when calculated using a correlation, that tend to underestimate the energy lost by the plate and thus must be experimentally determined to ensure with correlation is the best for the solar collector.

The model tends to estimate a higher temperature on the plate, which reduces the heat transferred to the C-P space and to the fluid in the pipes. Consequently, the simulated temperature in the tubes is lower than that observed experimentally.

Nomenclature

T	Temperature K
p	Pressure, Pa
d	aluminum thickness, m
b_1,b_2	Height and width of the tubes, m
Cp	Specific heat capacity, $Jkg^{-1}K^{-1}$
h_v	Latent heat of evaporation, Jkg^{-1}
I(t)	Solar irradiation, Wm^{-2}
κ	Dilatational viscosity, $kgm^{-1}s^{-1}$
h	Heat transfer coefficient, $Wm^{-2}K^{-1}$
D	Equivalent diameter, m
Greek letters	
α	Absorptivity
σ	Stefan Boltzmann constant, $Wm^{-2}K^{-4}$
ρ	Density, kgm^{-3}
ε	emissivity,m^3m^{-3}
τ	Transmissivity
μ	Viscosity, kg $m^{-1}s^{-1}$
Subscripts	
p	absorbed plate
f	air fluid
c	glass cover
0	ambient
a	Air
r	Radiation
Vectors and matrices	
$\mathbf{u}$	Velocity, m/s
$\mathbf{k}$	Thermal conductivity, $Wm^{-1}K^{-1}$
$\mathbf{I}$	Identity matrix
$\mathbf{n}$	Normal vector

References

Alleyne, F. S., Milczarek R.R. (2015). Design of Solar Thermal Dryers for 24-Hour Food Drying. Pp. 0-3 en *Proceedings of the 2015 COMSOL.*

Al-Tabbakh, A. A. (2022). Numerical Transient Modeling of a Flat Plate Solar Collector. *Results in Engineering* 15:100580. doi: https://doi.org/10.1016/j.rineng.2022.100580.

Azeez, K., Riyadh I. A., Zain A. O., Itimad D. J. A. (2023). Heat transfer enhancement and applications of thermal energy storage techniques on solar air collectors: A review. *Journal of Thermal Engineering* 9(5):1356-71.

doi: https://doi.org/10.18186/thermal.1377246.

Bakari, R. (2018). Heat transfer optimization in air flat plate solar collectors integrated with baffles. *Journal of Power and Energy Engineering* 06(01):70-84. doi: https://doi.org/10.4236/jpee.2018.61006.

Bakari, R., Rwaichi J. A. M., Karoli N. N. (2014). Effect of glass thickness on performance of flat plate solar collectors for fruits drying. *Journal of Energy* 2014:1-8. doi: https://doi.org/10.1155/2014/247287.

Bensaci, C. E., Abdelhafid M., Sánchez de la Flor F.J., Rodríguez Jara E., Rincón-Casado, A., Ruiz-Pardo A. (2020). Numerical and experimental study of the heat transfer and hydraulic performance of solar air heaters with different baffle positions. *Renewable Energy* 155:1231-44. doi: https://doi.org/10.1016/j.renene.2020.04.017.

Bolaji, B. O. (2012). Theoretical and Experimental Analyses of Heat Transfer in a Flat-Plate Solar Collector Design and Performance Evaluation of a Mobile Cooler Refrigerator Retrofitted with R134a View project Evaluation of Water-Extract from Fermented Ground Maize for its Potentials as Coolants for Engine and Machining Operations View project. doi: https://doi.org/10.2004/wjst.v9i3.227.

Gopi, R., Ponnusamy P., Fantin Arokiaraj A., Raji A. (2020). Performance comparison of flat plate collectors in solar air heater by theoretical and computational method. *Materials Today: Proceedings*, 39, 823-826.

Jallut, C., Jemni A., Lallemand M. (1988). Steady-state and dynamic characterization of an array of air flat-plate collectors. *Solar & Wind Technology* 5(5):573-79. doi: https://doi.org/10.1016/0741-983X(88)90049-5.

Kramer, K., Mehnert S., Geimer K., Reinhardt M., Fahr S., Thoma C., Kovacs P., Ollas P. (2017). Guide to standard ISO 9806:2017 a resource for manufacturers, testing laboratories, certification bodies and regulatory agencies. doi: https://doi.org/10.13140/RG.2.2.30241.30562.

Kumar, P., Singh D. (2020). Advanced technologies and performance investigations of solar dryers: A review. *Renewable Energy Focus* 35:148-58. doi: https://doi.org/10.1016/j.ref.2020.10.003.

Lingayat, A. B., Chandramohan V. P., Raju V. R. K., Meda V. (2020). A review on indirect type solar dryers for agricultural crops-Dryer setup, its performance, energy storage and important highlights. *Applied Energy* 258.

Mahroug, I., Doppiu S., Dauvergne J.L., Echeverria M., Toutain J., Palomo del Barrio E. (2021). Study of peritectic compound Li4(OH)3Br for high temperature thermal energy storage in solar power applications. *Solar Energy Materials and Solar Cells* 230. doi: https://doi.org/10.1016/j.solmat.2021.111259.

Matsumoto, Y., Valdés M., Urbano J.A., Kobayashi T., López G., Peña R. (2014). Global solar irradiation in north Mexico city and some comparisons with the south. *Energy Procedia*. Vol. 57. 1179-88.

Messina, S., González F., Saldaña C., Peña-Sandoval G.R., Tadeo H., Juárez-Rosete C.R., Nair P. K. (2022). Solar powered dryers in agricultural produce processing for sustainable rural development worldwide: A case study from Nayarit-Mexico. *Cleaner and Circular Bioeconomy* 3:100027. doi: https://doi.org/10.1016/j.clcb.2022.100027.

Mohana, Y., Mohanapriya R., Anukiruthika T., Yoha K. S., Moses J. A., Anandharamakrishnan C. (2020). Solar dryers for food applications: Concepts, designs, and recent advances. *Solar Energy* 208:321-44.

Mota, F. A. S., Furtado A. S. S., Leitao A. B. V., Medeiros N. C., Pereira G. S., Almeida M. N., Oliveira A., Oliveira M. M., Caselli F. T. R. (2025). Obtention of Methyl Esters Fractions through Distillation and Pour Point Evaluation of the Obtained Fractions. *Revista Mexicana de Ingeniería Química* 24(1). https://doi.org/10.24275/rmiq/IE24221

Ndukwu, M. C., Ibeh M., Okon B.B., Akpan G., Kalu C. A., Ekop I., Nwachukwu C.C., Abam F. I., Lamrani B., Simo-Tagne M., Ben A.E., Mbanasor J., Bennamoun L. (2023). Progressive review of solar drying studies of agricultural products with exergoeconomics and econo-market participation aspect. *Cleaner Environmental Systems* 9.

Rajarajeswari, K., Alok P., Sreekumar A. (2018). Simulation and experimental investigation of fluid flow in porous and non-porous solar air heaters. *Solar Energy* 171:258-70. doi: https://doi.org/10.1016/j.solener.2018.06.079.

Rani, P., Tripathy P. P. (2020). Thermal characteristics of a flat plate solar collector: influence of air mass flow rate and correlation analysis among process parameters. *Solar Energy* 211:464-77. doi: https://doi.org/10.1016/j.solener.2020.08.057.

Ranmode, V., Manmeet S., Bhattacharya J. (2019). Analytical formulation of effective heat transfer coefficient and extension of lumped capacitance method to simplify the analysis of packed bed storage systems. *Solar Energy* 183:606-18. doi: https://doi.org/10.1016/j.solener.2019.03.066.

Romero-Bonilla, H. I.; Jaramillo-Guanolique, A., Zambrano, C., Rios-Hidalgo, M., Solano-Maza, L., Choez-Tobo, C. (2025). Cocoa shell biochars for sustainable biodiesel production in Ecuador. *Revista Mexicana de Ingeniería Química* 24 (1). https://doi.org/10.24275/rmiq/IE24221

Rouissi, W., Naili N., Jarray M., Hazami M. (2021). CFD numerical investigation of a new solar flat air-collector having different obstacles with various configurations and arrangements. *Mathematical Problems in Engineering* 2021. doi: https://doi.org/10.1155/2021/9991808.

Shahsavari, A., Akbari M. (2018). Potential of solar energy in developing countries for reducing energy-related emissions. *Renewable and Sustainable Energy Reviews* 90:275-91.

Tiwari, R., Mishra K., Nath G. (2011). Advanced renewable energy sources. *Advanced Renewable Energy Sources*. Vol. 1. 45-109.

Vivekanandan, M., Jagadeesh D., Natarajan A., Mohan N., Dineshkumar M. (2020). Experimental and CFD investigation of fully developed flow solar air heater. *Materials Today: Proceedings*. Vol. 37. 2158-63.

Xiao, S., Zhang Y., Xia K., Long J. (2022). Influence of operating conditions on solar energy utilization efficiency of flat plate solar collector. *Renewables: Wind, Water, and Solar* 9(1). doi: https://doi.org/10.1186/s40807-022-00070-9.